Soft Matter

Accepted Manuscript

ROYAL SOCIETY OF CHEMISTRY

www.rsc.org/softmatter

Confronting the Complexity of Carbon Nanotube Materials †

Fernando Vargas-Lara[*a] **and Jack F. Douglas**[*a]

The morphology of commercially available carbon nanotube materials is often much more complex than the term "carbon nanotube" (CNT) would imply. Commercial CNT materials are typically composed of roughly spherical CNT domains having a highly ramified internal structure and a size on the order of microns. Clearly, such structures cannot reasonably be modeled as "rods". To address this problem, we first perform molecular dynamics simulations (MD) to generate structures similar to those measured experimentally, based on the presumptions that CNT domains are composed of worm–like cylinders having observed persistence lengths and that these CNTs are confined to spherical domains having the observed average domain size. This simple model generates structures remarkably similar to those observed experimentally. We then consider numerical path–integral computations to calculate the self–capacitance C and intrinsic conductivity $[\sigma]_\infty$ of these CNT rich domains. This information is then incorporated in a generalized effective medium theory to estimate the conductivity of bulk composite materials composed of these complex–shaped "particles". We term these CNT structures "tumbleweeds", given their evident morphological similarity to this naturally occurring growth form. Based on this model, we find that the conductivity percolation threshold of the tumbleweeds can be quite low, despite their quasi–spherical average shape. We also examine the structure factor $S(q)$ of the CNT–rich domains as function of the number N of CNTs within them, and the overall domain size to aid in the structural characterization of CNT nanocomposites. The structure factor $S(q)$ of our model tumbleweed is found to resemble that of hyperbranched, star and dendrimer polymers, and also domain structures observed in polyelectrolytes. Commercial CNT materials at high loading should then have physical features in common with suspension of "soft" colloidal particles by virtue of their deformability and roughly spherical shape.

Adding carbon nanotubes (CNTs) to polymeric materials can enhance their viscosity and mechanical strength[1], as well as electrical[2,3] and thermal conductivity[4]. It is generally appreciated that these property changes depend strongly on the structural parameters of the individual CNTs, such as their shape (e.g., CNT persistence length or other measure of CNT undulation scale), length, or diameter, as well as their degree of dispersion in the polymeric matrix[5]. While it is possible to synthesize long and relatively straight CNTs[6], and even to separate single wall CNT by length[7] and chirality[8], commercial CNT materials produced by chemical vapor deposition (CVD) are commonly composed of CNT–rich domains having a highly irregular internal structure[9–11]. It is often unclear whether these are aggregated CNTs having a worm–like cylinder morphology or are instead inherently branched carbon materials as found with carbon black[12]. CNT branching has been directly observed by transmission electron microscopy in CVD growth of CNT in association with fission of the catalytic nanoparticles[13], leading to a hierarchy of CNT diameters as in the formation of branches in plants. The buildup of amorphous carbon probably also acts to "cross–link" the CNTs. The as–received commercial material normally contains nodular sub–structures that progressively are broken down into isolated domains and CNT fragments under aggressive processing conditions aimed at dispersing these structurally complex materials[10]. This "tumbleweed" morphology is the reality of most commercially available in CNT materials[9,10] and we directly address what properties derive from them without judgment about whether such structures are "better" or "worse" than the ideal rod dispersions often invoked to explain the properties of CNT polymer nanocomposites.

In contrast with most theoretical[14] and experimental[3,15,16] studies that assume perfectly dispersed CNTs modeled as rods, we explore how the addition of tumbleweed CNT domains affects the conductivity of composites containing them. In particular, we approach the calculations of the properties of composites filled with these complex–shaped particles based on the same type of continuum theory developed by Einstein[17] and Maxwell[18] for calculating the viscosity and the electrical conductivity of rigid and conductive spheres, respectively, dispersed at low concentrations within a fluid or insulating matrix materials, respectively. Unfortunately, the extension of such calculations to describe particles having other shapes is a highly non–trivial problem and analytic calculations are restricted to ellipsoids and a few other mathematically tractable forms[19]. The present work utilizes a highly accurate computational method for calculating the leading virial coefficient for the viscosity and electrical conductivity for essentially *any* particle shape[20,21]. In particular, the numerical

† Electronic Supplementary Information (ESI) available: [Attached PDF file]

[a] *Materials Science and Engineering Division, National Institute of Standards and Technology, Gaithersburg, MD, 20899, USA; E-mail:luis.vargas@nist.gov; jdouglas@nist.gov*

path–integration method ZENO[22] calculates the intrinsic conductivity $[\sigma]_\infty$, which represents the leading term in the virial series expansion for the conductivity of the composite σ,

$$\sigma = \sigma_{\rm pol}\left[1 + [\sigma]_\infty \phi + O\left(\phi^2\right)\right], \qquad (1)$$

where ϕ is the concentration of conductive nanoparticles to a non–conductive polymeric matrix having a conductivity, $\sigma_{\rm pol}$.

The basic principle underlying the ZENO program is that the Laplacian operator has a fundamental relation to random walks, as expressed in the diffusion equation and many of the problems of mathematical physics can be recast computationally by generating random walks and calculating appropriate averages defined by these paths as they sample space[23]. The validation at this path–integration method against existing exact results for relatively simple objects has been extensively considered in prior work where it has been established that the properties that we consider in this paper can be calculated to an uncertainty[21] of $\approx 1.5\%$ and an accuracy of similar order in cases where exact results are known. The path–integral method is also much faster and does not involve the difficult problem of meshing boundaries of complex shaped particles. At present, the path–integral method is the only existing computational method of sufficient computationally efficiency to address the difficult problem of calculating electrostatic and hydrodynamic transport properties for such a large collection of complex–shaped particles as required in the present problem. Specifically, in addition to $[\sigma]_\infty$, the path–integration method method allows for the determination of the electrostatic capacity C to high accuracy and precise estimation of the particle hydrodynamic radius $R_{\rm H}$, regardless of particle shape complexity[21].

For specificity, we know from elementary electromagnetism that the electrostatic capacity C of a conductive spherical particle with respect to an electrode at infinity ("self–capacity") equals $C = 2\pi\epsilon R$, where ϵ is the permitivity of space and R is the sphere radius. From Maxwell[18], the leading conductivity virial coefficient for a conductive sphere equals $[\sigma]_\infty = 3$ and Einstein's[17] corresponding result for the viscosity of a suspension of rigid particles equals, $[\eta] = 5/2$. Pólya and Szegő [24] have discussed attempts to extend such calculations to other shapes and the great difficulties involved in even making rough numerical estimates of these "shape functionals". The path–integral computational program ZENO[22] should then be a powerful tool in calculating the properties of mixtures containing complex–shaped particles such as tumbleweed CNT domains, or other nanoparticles and polymers needing characterization for nanotechnology applications.

Before initiating our calculations, we need to explain our assumptions regarding how we model CNT tumbleweed domains and the property calculations of composites containing these complex–shaped particles. First, as conventional in the modeling of polymers in solution[28], we adopt a continuum approach so that we neglect any intrinsic change in the polymer matrix molecular dynamics arising from alterations in the entanglement or glass–formation physics through the introduction of particles in the polymer matrix[29]. There is some validation of this continuum approach for polymeric materials through molecular dynamics simulations (MD) of untangled polymer fluids with nanoparticle additives having different shapes[30,31], but more studies over a range of particle concentrations would be helpful.

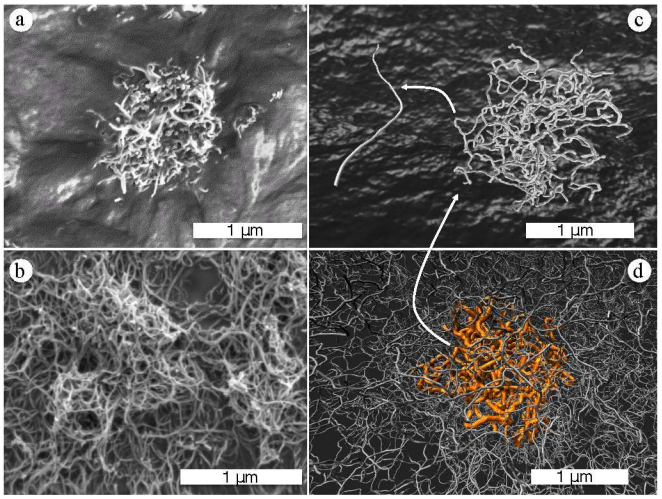

Figure 1: Observed and simulated CNT "tumbleweed" domains. a) An isolated CNT domain within an epoxy sample obtained by scanning electron microscopy imaging of fractured nanocomposite samples. (See Ref. 25 to appreciate the similarities in shape between these CNT domains and real tumbleweeds and accordingly we term them CNT "tumbleweeds"); b) CNT morphology of a relatively high concentration CNT sample in an epoxy matrix where the epoxy has been etched away with ultraviolet radiation before imaging[26]. Both CNT samples are commercial materials and these morphologies are rather typical of this class of materials[10]. c) A simulated CNT tumbleweed confined to a sphere. d) At high CNT concentrations, where a tumbleweed "gel" is obtained, each tumbleweed loses its identity in the melt of other tumbleweeds. (This phenomena is also found in accumulations of real tumbleweeds[27].) For visualization purposes, an individual tumbleweed is colored in orange. This tumbleweed is formed by 32 CNTs, where each CNT has a representative length $L \approx 2\ \mu m$.

To simplify our calculations for the CNT tumbleweeds, we adopt two approximations. First, we assume that the particles are isotropically distributed in their orientation in our calculation of $[\sigma]_\infty$. This is a reasonable approximation given the roughly spherical shapes of the CNT tumbleweeds (See Figure 1). Second, measurements have established that multi–wall CNTs have an electrical conductivity that is essentially *infinite* in comparison to the polymer matrix to which they are added[3]. This high conductivity contrast allows us to ne-

glect conductivity differences that might arise from conductivity variations in the individual CNT domains. However, this assumption is probably not generally appropriate for single walled CNTs were chirality can have a large influence on the CNT conductivity, at least at high frequencies[32]. Consequently, we do not claim to model single–wall CNT materials, but rather focus on commercial CNT materials normally composed of multi–wall CNTs.

The assumptions of isotropy with respect to the particle orientation and a high contrast in electrical conductivity $\Delta = \sigma_{\rm CNT}/\sigma_{\rm pol}$, specifically the ratio of the electrical conductivity of the particle $\sigma_{\rm CNT}$ to the electrical conductivity of pure matrix material $\sigma_{\rm pol}$ to which the particle is added, reduces the exact calculation of $[\sigma]_\infty$ to the determination of the trace of the electrical polarizability tensor $\boldsymbol{\alpha_e}$ of the conductive tumbleweed particles[33],

$$[\sigma\,(\Delta \to \infty)] \equiv [\sigma]_\infty = \langle \boldsymbol{\alpha_e} \rangle / V_{\rm CNT}, \qquad (2)$$

where $\langle \boldsymbol{\alpha_e} \rangle = (1/3)\,trace\,(\boldsymbol{\alpha_e})$, and $V_{\rm CNT}$ is the volume of the CNT. In the more general case in which the particles are not isotropically distributed, the determination of $[\sigma]_\infty$ involves an averaging with respect to the components of $\boldsymbol{\alpha_e}$. Martin and coworkers[34,35] have recently considered this situation for oriented sheet–like conducting nanoparticle additives where the calculation of σ requires a different weighting of the polarizability components, a generalization easily considered in our computational method. These particle orientational effects should be less important in tumbleweed structures than in rod–like or sheet particle dispersions where changes in processing conditions can induce significant particle orientation and macroscopic property anisotropy in some cases. Of course, the tumbleweeds should be less prone to this effect and this might be a great advantage for this class of disordered CNT materials.

There are two further physical ingredients that we need for modeling the CNT tumbleweed domains and σ of nanocomposites made from adding these particles to a polymeric matrix. First, we need to generate physically reasonable representations of these structures on which our path–integral calculations can be applied. We adopt a coarse–grained model of the CNT domains drawn from the field of polymer science where structures having the same geometry arise. In particular, past experiments on fragment CNT materials in the form of isolated segments have established that these CNT can be modeled as worm-like tubes[36,37]. It is apparent also from observation of the CNT material before it has been mechanically broken down under CNT shear stress or some other mechanical or chemical degradation process that the CNT are localized into roughly spherical domain structures that slowly disintegrate under prolonged applied stress[10]. For typical processing times these clusters survive as the predominant structures within the nanocomposite, along with the CNT segments broken from the surface of these objects. We then introduce a "standard" polymer model that generates worm–like tubular CNT configurations confined to a finite tumbleweed domain as a reasonable generic model for these complex structures. Since we are treating this problem from a continuum theory of conductivity, the interaction between the CNT with the polymer matrix or between the CNTs has only a secondary significance. The results of this model are validated by comparison of the simulated tumbleweed structures to representative images of the real CNT materials used in commercial applications.

Finally, we must adopt a model for estimating the conductivity of composite materials made from such complicated–shaped particles. We approach this problem through the use of an effective medium theory, and we utilize, in particular, the "generalized effective medium theory" (GEM)[38] since this model has performed well in previous studies of polymer nanocomposites containing CNTs[3]. This model is known to be useful for estimating the conductivity of composites containing complex–shaped conducting particles, but the conductivity percolation threshold is normally adjusted empirically in this model because it has not been possible before to calculate $[\sigma]_\infty$ for complex–shaped particles As we shall illustrate below, the conductivity virial coefficient $[\sigma]_\infty$ *fixes* the conductivity percolation concentration $\phi_{\rm c}$ in GEM theory. Since we can calculate $[\sigma]_\infty$ precisely for *any* particle shape with our path–integral program (ZENO), we can now make estimates of the conductivity of dispersions of highly conductive particles based on GEM theory. The modeling of σ at high filler concentrations is subject to the limitations of this effective medium theory, but allows us to model σ without free parameters. We next describe our MD–generated CNT tumbleweeds based on the model described above, implement the calculation of C and $[\sigma]_\infty$ by applying path–integration methods to 10^3 ensembles of tumbleweed domains generated by MD. Finally, we calculate the conductivity of composites of CNT tumbleweeds based on GEM theory in conjunction with our path–integral calculations of $[\sigma]_\infty$.

Our paper is summarized as follows. In Section 1, we describe the molecular model utilized to generate CNT domains having tumbleweed–like morphologies. In Section 2, we calculate the the electric properties of the tumbleweeds, i.e., C and $[\sigma]_\infty$, as well as σ of composites made with these complex–shaped particles. In Section 3, we present the structure factor of the tumbleweeds and shape–related properties that should be useful in the experimental characterization of these structures. Finally, we conclude in Section 4 .

1 Molecular Model to Generate CNT Tumbleweed Morphologies

There is currently limited understanding of the relevant factors controlling the growth of tumbleweed domains and measurements of the branching characteristics and other topological properties of these clusters are limited. Under these circumstances, we adopt a tentative coarse–grained model intended to capture the main physical characteristics of these clusters, an approach validated by comparing the structure generated with these observed in high resolution imaging and scattering studies of these structures.

For the MD simulation part of our work, each individual CNT is represented by a worm–like cylinder model[39], as illustrated in Figure 1 (c). As noted above, this is a physically established model for the observed fragments of both single and multi–wall CNT materials[36,37]. The high polarizability of CNT materials makes the fundamental derivation of a intermolecular potential describing the interactions between the CNT segments extremely difficult and the deduction of such potentials is further complicated by chemical methods used to clean the CNT to various degrees that alter the surface chemistry and thus the interaction potential. Embedding the CNT in a polymer matrix further alters this effective interaction. Given this complex situation, we adopt the procedure that we, and others, have used in modeling DNA (another structure that described by a worm–like chain) in solution where hydration, polarizability, and charge condensation greatly complicate the modeling of the intermolecular interaction. In particular, we simply model the collective short–range interaction by a truncated 12–6 Lennard–Jones potential (LJ),

$$U_{\rm LJ}^{12-6}(r) = 4\epsilon_{\rm LJ}\left[\left(\frac{\sigma_{\rm LJ}}{r}\right)^{12} - \left(\frac{\sigma_{\rm LJ}}{r}\right)^{6}\right] \qquad r < 2^{1/6}\sigma_{\rm LJ}, \tag{3}$$

where $\varepsilon_{\rm LJ} = 1.0$ is a phenomenological measure of the short–range interaction strength and $\sigma_{\rm LJ} = 1.0$ defines the diameter of the CNT. Again drawing on this analogy with DNA structure, we model the chain by a finitely extensible, nonlinear elastic (FENE) anharmonic–spring potential,

$$U_{\rm FENE}(r) = -\frac{kR_0^2}{2}\ln\left[1 - \left(\frac{r}{R_0}\right)^2\right]. \tag{4}$$

Here, $k = 30\ \epsilon_{\rm LJ}/\sigma_{\rm LJ}^2$ and $R_0 = 1.5\ \sigma$ are the bond strength and maximum bond length, respectively. In order to mimic the multi-walled CNT morpholgies commonly found experimentally such as in Ref. 36, we map $\sigma_{\rm LJ}$ with the outer CNT diameter having a typical value of $\sigma_{\rm LJ} = 21$ nm, and we consider CNTs formed by a number of beads n, with $n = 100$ or 200 ($L \approx 2\ \mu$m or $4\ \mu$m in length). Additionally, to model the bending stiffness of these multi–walled CNTs, we assume the connecting beads in each CNT interact via a bending potential,

$$U_{\rm lin}(\theta) = 9\ \epsilon_{\rm LJ}[1 - \cos(\theta)], \tag{5}$$

where θ is the angle formed by three consecutive beads yielding CNTs with a static persistence length $l_{\rm ps} = 200$ nm. An average density $\rho_{\rm CNT} = 1.726\ {\rm g/cm^3}$ of multi–walled CNTs [40] implies that each bead has an average mass $m_{\rm bead} = 4.85 \times 10^{-18}$g. In this way, we generate worm–like cylinders having the observed persistence length of multi-walled CNTs as the basic primary unit of our CNT domain structures.

To simulate the observed roughly spherical "tumbleweed" CNT domains (see Figure 1), we consider the CNT to be constrained to lie inside a spherical shell of radius R on the order of 1 μm. The CNT–shell interaction is modeled for simplicity by a 9–3 LJ potential,

$$U_{\rm LJ}^{9-3}(r) = \epsilon_{\rm LJ}\left[\frac{2}{15}\left(\frac{\sigma_{\rm LJ}}{r}\right)^{9} - \left(\frac{\sigma_{\rm LJ}}{r}\right)^{3}\right] \qquad r < (2/5)^{\frac{1}{6}}\ \sigma_{\rm LJ}, \tag{6}$$

but almost any short range potential would serve to create the desire effect of creating spherical diffuse domains of CNT in the form of a diffuse domain containing CNTs. We vary the number N of CNTs inside our model spherical tumbleweed domains (see Figure 1 (c)) as $N = 1, 2, 5, 10, 20, 32, 64, 128$ or 256. Figure 1 (d) shows a concentrated CNT material formed by a collection of tumbleweeds (See conclusions). All the MD simulations were performed at a reduced temperature $T/\epsilon_{\rm LJ} = 1.0$ for $\geq 10^7$ time steps using LAMMPS[41].

We emphasize again that our MD simulations are performed only to create plausible realizations of the CNT tumbleweed domains and that these simulations are rather insensitive to our choice of potential parameters. The form of the intermolecular potential thus has little effect on the calculated transport properties based on continuum theory using ZENO and its extension using effective medium theory.

We report the average properties for each tumbleweed cluster. In particular, we sample 10^3 configurations once CNTs reach their thermal equilibrium state. The Monte Carlo path–integration program ZENO[21,22,33] allows for the computation of the conductive properties of the tumbleweed and the composite containing them. We consider a relatively large number of random paths $\geq 10^7$ for each property calculation to achieve uncertainty values smaller than the numerical data points reported in each figure. We fit the data using the software Grace[42] which considers the Levenberg–Marquardt algorithm. The uncertainties related to the fitting correspond to one standard deviation which are included on the figures only if this value is bigger than the symbol size. Visual Molecular Dynamics (VMD)[43] is used to visualize the CNT structures. Note the close similarities to the observed CNT tumbleweed domain to the simulated domain illustrated in Figure 1. Now that we can generate a reasonable facsimile of the CNT do-

mains, we now explore the electrical properties of these complex structures of relevance for applications.

2 Basic Conductivity Properties of Tumbleweeds

We first study the conductive properties of tumbleweed domains. Figure 2 (a) shows the capacitance C for a tumbleweed formed by a different N normalized by the self–capacitance of an individual CNT, C_1. In this figure, the red symbols indicate our computed values, and the solid line is a mean field theory[44–46] estimate of C for a tumbleweed CNT domain,

$$C = \frac{NC_1}{1 + NC_1/C^*}, \tag{7}$$

where C^* is the effective capacitance of the tumbleweed domain the limit of loading with many CNTs. We see that when N becomes larger than about 5, the capacity of the tumbleweed C no longer varies linearly in N and begins to vary more slowly, ultimately saturating to C^*.

The same crossover expression as in Eq. (7) arises in the related problem of hydrodynamic screening of the friction coefficient f of flexible polymer chains where to the radius of gyration of the polymer chain replaces C^* for the tumbleweed[45] and C_1 corresponds to the friction coefficient of a polymer segment[45,47]. This "screening" or "homogenization" transition is also well known in electromagnetic scattering phenomena[48], electrostatics[49], and especially in a biological context where C is proportional to the Smoluchowsky rate constant for diffusion–limited reactions which is important for understanding ligand binding [50] or the evaporation efficiency of the stomata pores of leaves[51], and other important biological phenomena. Douglas et al. discusses some of these and other applications of C in Ref. 45.

We see that C of the tumbleweeds reflects the additive contribution of the CNTs when N is small, but C approaches a constant C^* for large N as a consequence of a screening transition associated with the overlap of the potential fields of the CNTs within the tumbleweed domain. The inset to Figure 2 (b) shows the average magnitude of the electric polarizabilty tensor $\langle \boldsymbol{\alpha}_\mathbf{e} \rangle$ of the tumbleweed domains exhibits a similar screening effect so that $\langle \boldsymbol{\alpha}_\mathbf{e} \rangle$ also approaches the polarizability of a conductive sphere for large N where the saturation effect again becomes prevalent near $N = 5$. The exact crossover value of N depends on the structural properties of the individual CNTs. The important point here is that N is not a large number. The solid line in the inset corresponds to the relation,

$$\langle \boldsymbol{\alpha}_\mathbf{e} \rangle = \frac{f(N) \langle \boldsymbol{\alpha}_\mathbf{1} \rangle}{1 + f(N) \langle \boldsymbol{\alpha}_\mathbf{1} \rangle / \langle \boldsymbol{\alpha}^* \rangle} \tag{8}$$

where $f(N) = N + 2.75\left(N^{3/4} - 1\right)$ includes subdominant

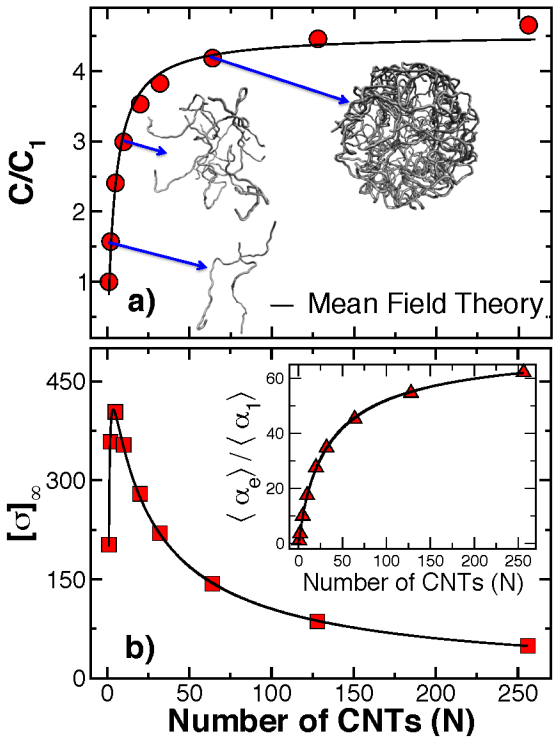

Figure 2: Capacitance C and intrinsic conductivity $[\sigma]_\infty$ of tumbleweeds formed by a different N. a) C normalized by the capacitance of one CNT C_1 [21]. The insets are snapshots taken from representative tumbleweed configurations. b) $[\sigma]_\infty$ reaches its maximum value at a relative low number of CNTs $N \approx 5$. The inset shows the normalized average magnitude of the electric polarizabilty tensor $\langle \boldsymbol{\alpha}_\mathbf{e} \rangle / \langle \boldsymbol{\alpha}_\mathbf{1} \rangle$, where $\langle \boldsymbol{\alpha}_\mathbf{e} \rangle$ and $[\sigma]_\infty$ are related via $[\sigma]_\infty = \langle \boldsymbol{\alpha}_\mathbf{e} \rangle / V_\mathrm{N}$. Here V_N is the volume of the CNT domains. The symbols are our computed values and the line is a mean field prediction from Eq. (7) and (8), for panels a) and b), respectively.

corrections to the leading N scaling and $\langle \boldsymbol{\alpha}_\mathbf{1} \rangle$, $\langle \boldsymbol{\alpha}^* \rangle$ are the electric polarizability tensor of a single CNT and a conductive sphere containing the CNT, respectively.

The intrinsic conductivity $[\sigma]_\infty$, which exactly determines the material conductivity at low additive concentrations (see Eq. (1)), is calculated using ZENO and the results are presented in Figure 2. We see that $[\sigma]_\infty$ exhibits a sharp peak around $N = 5$, the crossover value of N noted above for C and $\langle \boldsymbol{\alpha} \rangle$. Although the emphasis of the present paper is on the conductive properties of CNT tumbleweed domains, we note that the Stokes friction f is related to C as $f \approx 6\pi\eta C$, an approximation on the order of 1 % accuracy[21] and $[\sigma]_\infty$ is correspondingly proportional to the intrinsic viscosity $[\eta]$ to a good approximation[21,33] so that our calculations immediately provide estimates of the diffusion coefficient D and $[\eta]$ of the tumbleweeds suitable for comparison of solution mea-

surements on these commercial CNT materials.

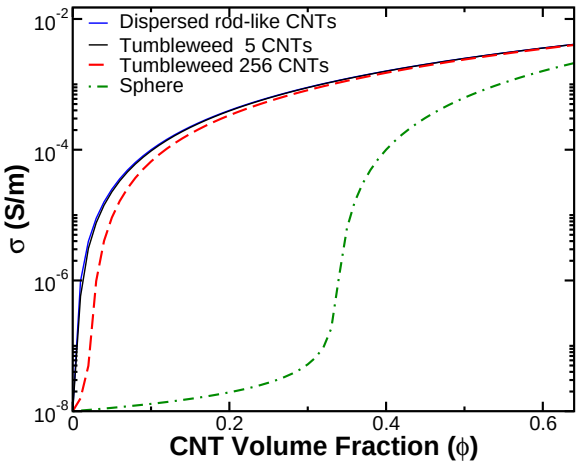

Figure 3: Generalized effective medium theory (Eq. (9)) estimates the conductivity σ for model CNT tumbleweeds composed of 5 and 256 CNTs. We compare these results also to those for a single conducting sphere having the same σ as the individual CNTs. We find that the CNT tumbleweed composites naturally have low percolation threshold ϕ_c on the order of 1 %, even though these particles are not rod–like. The concentration axis is truncated at the maximum value for the random close packing of hard spheres $\phi^* = 0.64$, which is also a reasonable estimate for the maximum concentration packing for flexible polymers[52]. Of course, this estimate of the maximum achievable concentration of CNT constitutes an upper bound of the CNT packing fraction.

Knowing $[\sigma]_\infty$ of the additive, we then estimate how the conductivity σ of a composite (at fixed frequency) changes as a function of ϕ using GEM theory[38],

$$(1-\phi)\,\frac{\sigma_{\rm epox}^{1/s}-\sigma^{1/s}}{\sigma_{\rm epox}^{1/s}+A\sigma^{1/s}}+\phi\,\frac{\sigma_{\rm CNT}^{1/t}-\sigma^{1/t}}{\sigma_{\rm CNT}^{1/t}+A\sigma^{1/t}}=0. \quad (9)$$

In this expression, we fix A by matching the mean field Bruggeman symmetric effective medium equation[38] to the exact virial expansion[19] for σ to obtain $A = ([\sigma]_\infty - 1)$, and $\sigma_{\rm epox}$, and $\sigma_{\rm CNT}$ are the conductivity of the CNTs, and epoxy matrix, respectively; s and t are the usual conductivity percolation exponents[53].

GEM theory is a hybrid model that incorporates ingredients of effective medium theory (a mean field theory) and exact scaling results found from percolation theory. As such, it provides one of the most predictive expressions to the conductivity and other nanocomposite properties containing complex–shaped particles. The detailed arguments on which this model is based are described in Ref. 38. In previous studies[3], GEM theory successfully described σ of single wall and multi–wall CNT filled–materials, having a rod–like morphology (such materials exist, but, as noted above, this is not the norm for commercial CNT materials[9,10]). We simply utilize this powerful framework with one important difference, we directly calculate the conductivity percolation threshold based on our ZENO calculation of $[\sigma]_\infty$. This is a new development introduced in this paper.

In Figure 3, we show the GEM model $\sigma(\phi)$ predictions for composites containing tumbleweeds formed by 5 and 256 CNTs. The tumbleweeds containing $N = 5$ CNTs give rise to a relative low percolation thresholds, $\phi_c \approx 1$ %, consistent in order of magnitude with conductivity measurements on multi–walled CNT composites in polypropylene[54] where the conductivity data was fit to the GEM equation under both quiescent and steady–shear conditions. Here, we chose the three dimensional values of the conductivity percolation exponents[53] $s = 0.73$, $t = 2.0$ and we take the contrast ratio[2,3] $\sigma_{\rm CNT}/\sigma_{\rm epox} = 10^6$. We further take $\sigma_{\rm CNT}$ to be the conductivity of the densest achievable packing of the CNT material, a property that depends strongly on the contact resistance between the tubes and, in particular, on the CNT defect density, surface chemistry, etc. This plateau value can apparently vary by orders of magnitude in CNT materials depending on how the CNT are fabricated and processed and in Figure 3 we chose representative values of $\sigma_{\rm CNT}$ for multi–walled materials that we have studied before at NIST[55]. Investigation of the physical factors controlling $\sigma_{\rm CNT}$ is an attractive topic for future investigations.

We see from Figure 3 that the conductivity percolation threshold ϕ_c can be small even if the CNTs are in the form of tumbleweed domains rather than dispersed rods. The key to a low ϕ_c in these particles is their diffuse polymeric structure and their corresponding high polarizability. Of course, the estimated ϕ_c is somewhat smaller if the CNT are actually dispersed in the form of randomly oriented and fully dispersed worm–like cylindrical structures. Taking a reasonable estimate for the persistence length and CNT diameter[36], as in our analysis above or the tumbleweed domains, we can also calculate ϕ_c using ZENO and GEM theory to get an estimate of the limiting ϕ_c that might be achievable in such ideal dispersions. Extending our calculations above to such model CNT structures indicates that ϕ_c can be quite small when the CNT are long. In particular, the GEM model predicts that ϕ_c (inflection point in Fig. 3) scales in inverse proportion to $[\sigma]_\infty$,

$$\phi_c \approx 1.6/[\sigma]_\infty, \quad (10)$$

which should apply to conducing particles of any shape. Since we find that $[\sigma]_\infty$ depends on the length L of the worm–like CNTs as,

$$[\sigma]_\infty \sim L^{0.9\pm0.05}, \quad (11)$$

we conclude that ϕ_c for worm–like CNT should scale as,

$$\phi_c \approx 4\,L^{-0.9\pm0.05}, \quad (12)$$

where L is in nm and we have taken the representative estimate of the static persistence length, $l_{\rm ps} = 200$ nm. (Mansfield and Douglas[44] previously investigated $[\sigma]_\infty$ for worm–like cylinders as a model of CNTs where the diameter and the length of the CNTs were varied over a wide range of values). However, this work did attempt neither to calculate the conductivity percolation thresholds based on this information nor estimate the conductivity of nanocomposites made of these type of particles). For L on the order of $O(1000\ nm)$, we then see that $\phi_{\rm c}$ is predicted to be very small, $\phi_{\rm c} \sim O(10^{-3})$, for such well–dispersed worm–like tube dispersion. We see, however, that $\phi_{\rm c}$ remains low and σ hardly changes for tumbleweeds containing 5 CNTs so the practical advantage of being "fully dispersed" CNTs is not really that great. Notably, the present method of calculations can be extended and applied to NPs having *any* prescribed shape.

A problem with such "ideal" CNT dispersed system is that it is hard to fabricate such materials in large enough quantities at a reasonable cost. Additionally, such systems have an inherent tendency to exhibit orientational ordering and bundling effects that can increase $\phi_{\rm c}$ substantially. The loss of stability of these dispersions over time and under temperature cycling can be expected to give rise to undesirable property changes in end–use applications, even if were possible to reproduce these materials and disperse them in polymer matrices in an economical fashion. The tumbleweed morphology should be relatively free of this type of "aggregation" problem and the roughly isotropic nature of the tumbleweed CNT domains should make them less prone to alignment by either electric or flow fields. Thus, the irregular form of these commercial CNT materials probably make these materials more desirable for some applications.

We are currently performing experiments at NIST to characterize the morphology and conductivity properties of CNT composites made from representative commercial CNT samples formulated into epoxy nanocomposites[?]. Preliminary measurements clearly indicated the presences of the isolated and roughly spherical tumbleweed structures within the composite whose number changes with concentration, but whose size has an invariant value of $\approx 2\ \mu m$. Conductivity measurements have revealed, as we predict, that the conductivity percolation threshold is very low $\approx 1\%$ in volume fraction for these nanocomposites, despite the absence of any appreciable amount of rod–like structures within the nanocomposites. Quantitative comparison with experiments will require high resolution imaging of the tumbleweed internal structures to determine the number of CNT in each domain, the nature of the branching involved, etc. For the present, we note that all the observation are qualitatively consistent with our model and we stress the need for better characterization of these structurally complex materials.

3 Structural Properties of Tumbleweeds

Scattering measurements provide a powerful experimental method for probing the internal structure of CNT materials. Unfortunately, there are no reliable models of the structure factor of complex polymer structures such as these that can be used to assess the geometry of these structures by neutrons, light and x–ray scattering measurements. Recent studies of CNT domains in polymer matrices by scattering have invoked multiple–parameter (as many as eight) models where the interpretation of the fit parameters is subject to rather large degree of uncertainty[9]. This situation is understandable since there is no reliable analytically–derived function for the structure factor for even randomly branched polymers (i.e., lattice animals or percolation clusters in three dimensions). The CNT domains are more complicated in that they do not have the simplifying feature of being fractal, which makes the problem of calculating their structure factor even more difficult from an analytic perspective.

We address this problem through a combination of model building and molecular dynamic simulations. In particular, we develop a numerical model for the static structure factor $S(q)$ for our tumbleweed structures where all the parameters of the model have a validated interpretation in terms of the real space structures generated by MD simulations. In this way, we quantify $S(q)$ of the tumbleweed domains in terms of physically meaningful parameters. This model seems to be applicable to a broad array of "fuzzy ball" polymer structures morphologically rather similar to our tumbleweed domains. We thus anticipate that our investigation of tumbleweed structures should find broad application in other areas.

We first explore how the CNT are distributed inside of the spherical shell by calculating the normalized density $\rho_{\rm n}(r)$ along the radial axis r, where $\int 4\pi r^2 \rho_{\rm n}(r)\ dr = 1$. Figure 4 (a) shows $\rho_{\rm n}(r)$ for tumbleweeds formed by a different number of CNTs (N). We find that the concavity of the density profiles $\rho_{\rm n}$ changes for tumbleweeds having $N \sim O(10)$ CNTs. A mathematical relation for $\rho_{\rm n}$ that describes all data from Figure 4 (a) to uncertainties ranging from $0.1\ \%$ to $6.5\ \%$ can be found in the electronic supplementary information (ESI).

We next compute the normalized static structure factor $S_{\rm n}(\vec{q}) = S(\vec{q})/n$ for tumbleweeds formed by a different number of CNTs (Figure 4 (b)). We compute $S(q)$ via the defining relation,

$$S_{\rm n}(\vec{q}) = \frac{1}{n^2}\left\langle \sum_{j=1}^{n}\sum_{k=1}^{n} \exp\left[i\vec{q}.\left(\vec{r}_j - \vec{r}_k\right)\right]\right\rangle. \qquad (13)$$

Here, $\vec{r}_j$ and $\vec{r}_k$ are the instantaneous coordinates of the beads, $\vec{q}$ the wave vector, and i is the imaginary number. For tumbleweeds domains containing more than 5 CNTs, $S_{\rm n}(\vec{q})$ begins to

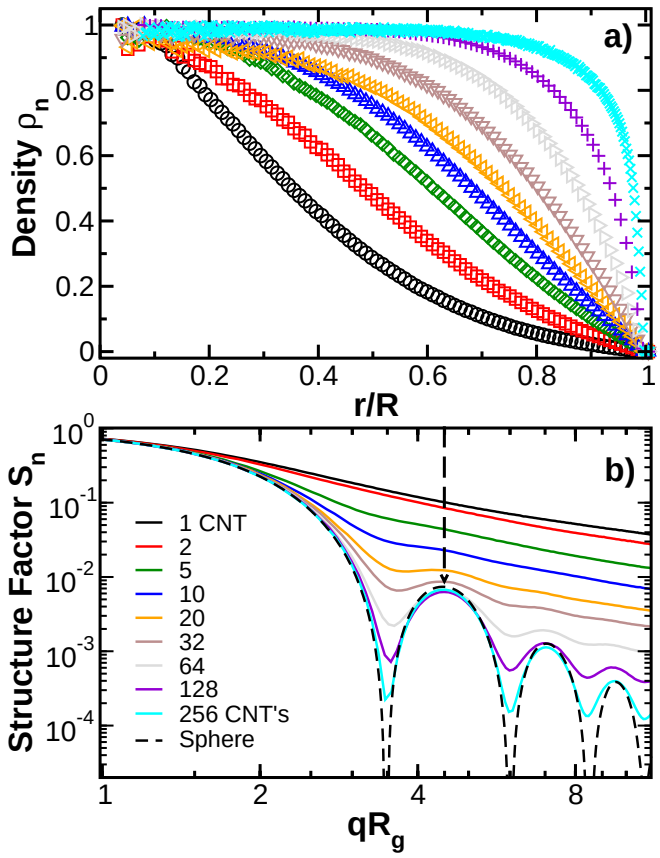

Figure 4: In a), the normalized density for tumbleweeds formed by a different number of CNTs (N). We find that the concavity of the density profiles $\rho_{\rm n}$ changes for tumbleweeds having $N > 5$, as in our observations of C and $[\sigma]_{inf}$ presented above. In b), the normalized structure factor $S_{\rm n}(\vec{q})$ of tumbleweeds formed by different number of CNTs. The $S_{\rm n}(\vec{q})$ profiles for tumbleweeds formed by more than 5 CNTs presents some shoulder formations which intensity increases with N. These features represent the transition from an elongated object to a more spherically symmetric one.

exhibit a shoulder, signaling the first emergence of a 'particle–like' structure. These features in $S_{\rm n}(\vec{q})$ also reflect a progressive transition shape from an anisotropic and diffuse structure to a compact roughly spherical structure.

Although we find that we cannot quantitatively compare our simulation estimates of $S(q)$ to existing scattering measurements on CNT polymer nanocomposites because of relatively limited structural characterization of this material and the length scales investigated in most of these measurements, the qualitative shape of $S(q)$ certainty accords qualitatively with observations on this class of materials. In particular, scattering measurements on single–walled CNT (SWCNT) materials normally indicate *no evidence* for the existence of rod structures in the material[56], even at high scattering wave–vector values q corresponding where one would expect a scaling of $S(q)$ inversely to q for rod–like particle additives. Chatterjee et al.[9] have further shown that suspensions of SWCNTs are also composed of order micron sized nodular domains with an internal structure that can be idealized as being "fractal" over a limited range of spatial scales with a fractal dimension (defined by the scaling $S(q) \propto q^{-d_{\rm f}}$) in the range between 2.2 ± 0.2 and 2.9 ± 0.1. Ultra–small angle neutron scattering (USANS) measurements should allow for the a probing of the SWCNT domains at larger length scales, but these measurements are yet not available for SWCNT composites. We conclude that a large body of scattering data on SWCNT materials[9,56–59] indicates that the primary structures of these SWCNT nanocomposites are normally more akin to random coil, or branched polymers having a fractal dimension $d_{\rm f}$ in a range between 2 to 3, rather than rod–like tubular structures having a fractal dimension near 1. This conclusion broadly accords with the basic physical picture of CNT materials advances for in the present work.

On the other hand, we focus in the present paper on commercially available multi–walled CNT (MWCNT) materials whose scattering properties are not obviously equivalent to those of SWCNT materials. Scattering studies of MWCNT materials are much more limited, but there is one study on this type of material by Sen et al.[60] that allows for a comparison of our predicted form of $S(q)$ to measurement. In the neutron measurements of Sen et al.[60], the MWCNTs were prepared by chemical vapor deposition of acetylene under different synthesis conditions such as variation catalysis type e.g., Ni, Co, Fe, catalysis concentration, synthesis temperature, etc. The MWCNT morphologies obtained in this study were also observed by using scanning electron microscope and these structures show a strong similarity to the experimental and simulation images shown in Fig. 1. SANS measurements were performed on these CNT samples over a relatively wide q range ($10^{-3} \leq q \leq 10^{-1}$ nm^{-1}) where there is no polymer matrix so that no background subtraction in the neutron scattering measurements is required for this data. A comparison of these observation with our $S(q)$ profiles is given in Fig. 5 (b), for representative diffuse tumbleweeds having $N = 10$, 20 or 32 CNTs. In both the experiments and simulations we see a Guinier–like decay of $S(q)$ at small q, whose decay length describes the average cluster size, followed by a limited q range over which an effective power–scaling is observed with an exponent between 2 to 3. At still higher q, $S(q)$ exhibits a shoulder feature in both the measurements and simulations, but the measurement uncertainties are larger in this high–q regime so we do not over interpret this feature. As a general observation, the approximate power–law scaling of $S(q)$ occurs over a much more limited range of q in the MWCNT materials, but otherwise the scattering data appears rather similar to obser-

vations on SWCNT materials. We look forward to comparing our model to neutron scattering measurements on materials that have been independently characterized by imaging studies to allow for more than a qualitatively validation of our model. In these future measurements, it will be important to determine, by direct imaging, that the tumbleweed domains have been dispersed in the polymer matrix since the overlap of these structures makes the interpretation of the scattering data somewhat complicated. We briefly discuss this more concentrated regime in Section 4.

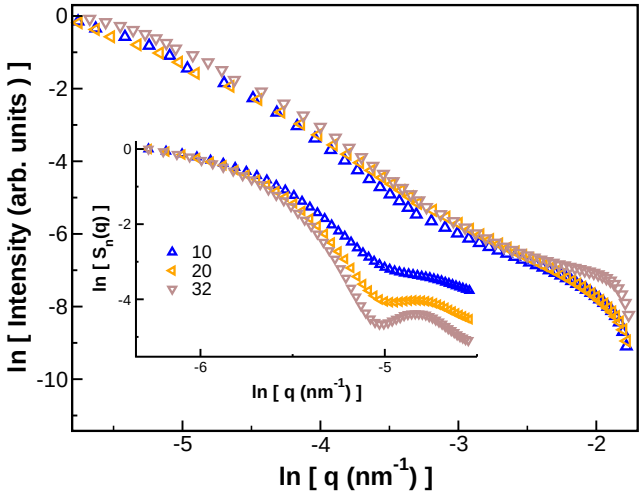

Figure 5: Small angle neutron scattering (SANS) measurements performed on multi–walled carbon nanotubes prepared by chemical vapor deposition of acetylene using different synthesis conditions (different colors)[60]. For comparison purpose, we include the structure factor obtained in this work for tumbleweeds having $N = 10$, 20 or 32 CNTs from Fig. 4 (b) as being representative. In both sets of data, we find qualitative similarities. A roughly Guinier decay of $S(q)$ at low q that defines the average cluster size, followed by a small effective power–law scaling over a limited q range with an effective power between 2 to 3. At high–q, $S(q)$ exhibits a shoulder feature, but data uncertainties are large in this q range.

We can alternatively characterize the tumbleweed domains in terms of other readily measurable properties, the hydrodynamic radius $R_{\rm H} = f/(6\pi\eta)$ and the radius of gyration $R_{\rm g} = \sqrt{\frac{1}{2n^2}\sum_{i,j} r_{ij}^2}$ of the tumbleweeds (Figure 6), where f is the friction coefficient of the tumbleweed, and η is the viscosity of the pure polymer fluid in which the tumbleweed are dispersed. The distance between particle i and j is labeled r_{ij}. $R_{\rm g}$ and $R_{\rm H}$ are perhaps the most basic measures of the size of polymeric structures from a measurement standpoint, based on static and dynamic scattering measurements.

The primary significance of ratio $R_{\rm H}/R_{\rm g}$ is as a descriptor

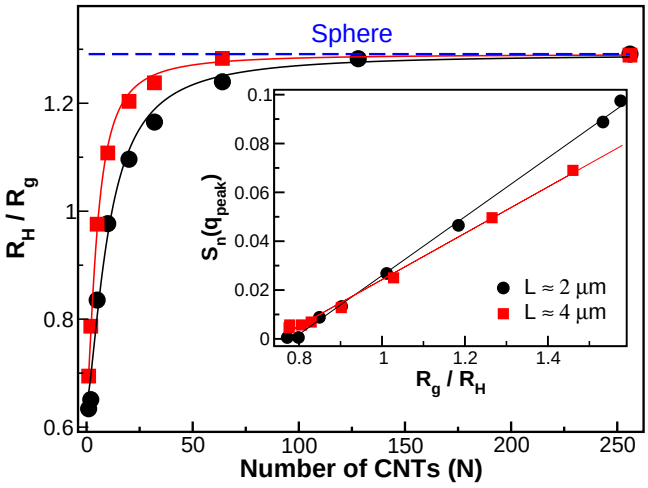

Figure 6: The ratio between the hydrodynamic radius $R_{\rm H}$ and the radius of gyration $R_{\rm g}$ for the tumbleweeds as a function of the number N of CNTs formed by $L \approx 2\ \mu m$ (in black) or $L \approx 4\ \mu m$ (in red). The symbols are the data and the solid lines correspond to fits to Eq. (14). The inset shows there is an strong correlation between $S_{\rm n}(q_{\rm peak})$ vs. $R_{\rm g}/R_{\rm H}$, where $S_{\rm n}(q_{\rm peak})$ represents the value of the structure factor at its first peak (See black arrow at Figure 4 (b)).

of molecular shape[61] and we can expect this ratio of properties to be useful for characterizing the CNT tumbleweeds since the shapes, and fluctuation in shapes of these structures, can be expected to change with the number of CNT within the domains, as in the case of star polymers where we have a transformation from anisotropic polymer shapes, as in the case of linear polymers, to a symmetric ball–like structure with an increase in number of arms. We expect, and indeed find, exactly this kind of shape transition in our simulated CNT tumbleweeds.

For spherical objects, $R_{\rm H}/R_{\rm g} = 1.291$, and for non–spherical ones, such as flexible polymer chains, we normally have $R_{\rm H}/R_{\rm g} < 1$. From Figure 6, we see that ratio saturates to value close to a sphere for $N \sim O(10)$, which agrees with the trend found in the $S_{\rm n}(\vec{q})$ data shown in Figure 4 (b). The inset in Figure 6 shows $(R_{\rm H}/R_{\rm g})$ vs. $S_{\rm n}(q_{\rm peak})$, where $S_n(q_{\rm peak})$ represents the value of the structure factor at its first peak (See black arrow at Figure 4 (b)). There is evidently a strong correlation between $S_{\rm n}(q_{\rm peak})$ and $(R_{\rm g}/R_{\rm H})$. In this figure, the black circles represent tumbleweeds formed by CNTs with $L \approx 2\ \mu m$ and the red squares with $L \approx 4\ \mu m$. The data has been fitted to the crossover equation,

$$\frac{R_{\rm H}}{R_{\rm g}} = \left(\frac{R_{\rm H}}{R_{\rm g}}\right)_{\rm Sphere}\left(1 - \frac{1/2}{1+\xi N^{3/2}}\right), \qquad (14)$$

where ξ is a fitting parameter, and $\xi = 0.03 \pm 0.02$ ($R^2 = 0.995$) or $\xi = 0.09 \pm 0.02$ ($R^2 = 0.999$) for $L \approx 2\ \mu m$ or

$L \approx 4\ \mu m$, respectively. We should then be able to characterize the CNT tumbleweeds though the measurement of $R_{\rm H}$ and $R_{\rm g}$, although the large size of these domains will require the estimation of these properties through particle tracking and imaging since the CNT domains are too large for routine scattering measurements.

4 Conclusions

We use MD simulations and path–integral methods to study the conductive properties of individual CNTs forming tumbleweed–like aggregates. We show that the capacitance C for these CNT rich domains rapidly approaches that of a conducting sphere due a screening transition so that the geometry and dispersion of the individual carbon nanotubes within the tumbleweed domains becomes essentially irrelevant after a relatively small number of tubes are within them. A simple mean field theory describes this transition in the scaling of C with the number N of CNTs within the tumbleweed domain. Additionally, we find the electric polarizabilty tensor $\langle \boldsymbol{\alpha}_{\mathbf{e}} \rangle$ of the tumbleweeds exhibits a similar screening transition, while their intrinsic conductivity $[\sigma]_\infty$ peaks at low concentrations of CNTs within the tumbleweed domains since this particle property corresponds to polarizability *per unit volume*. Evidently, there is an optimal number of CNTs to achieve the lowest percolation threshold for a fixed domain size, and this number corresponds to the N range in which we observe a screening transition in both C and $\langle \boldsymbol{\alpha}_{\mathbf{e}} \rangle$. We argue that dispersed rod–like CNTs are not necessary the optimal form of CNT additive for enhancing the conductivity of polymer materials if a low percolation threshold is not the only criterion for the utility of these materials. In particular, the high $\langle \boldsymbol{\alpha}_{\mathbf{e}} \rangle$ of the CNT domains makes the conductivity percolation threshold $\phi_{\rm c}$ low and their relatively symmetric geometrical form also makes them less susceptible to field–induced orientation. Thus, this relatively inexpensive CNT material is attractive in applications where property stability under high fields is required. We relate the change in the electric properties of the tumbleweeds to the static structure and experimentally accessible structural parameters such as $R_{\rm H}/R_{\rm g}$. We see that the screening transition in the tumbleweeds nearly coincides with a shape transition signaled by the condition, $R_{\rm H}/R_{\rm g} \approx 1$. Near this transition in geometry, the tumbleweed domains are geometrically diffuse, but relatively symmetric objects of high polarizability, ideal structures for certain applications.

Our investigation of CNT composites has mainly focused on the "dilute" regime, where the tumbleweed domains exist in relative isolation, a limit that simplifies the characterization of these structures from imaging and scattering measurements. As a tentative assumption, we took the tumbleweed to have a fixed domain size based on observational data suggested, but that assumption should be carefully assessed as the model is refined in the future. At higher concentrations of these complex–shaped particles, we expect these branched polymeric structures to interpenetrate and lose their identity, i.e., the individual tumbleweeds are no longer visually discernible because of their interpenetration. In solutions of flexible linear polymers, this "disappearing act" makes the osmotic pressure, and other properties such as the collective diffusion coefficient and Soret coefficient insensitive to polymer chain mass, a physical effect that implies a non–trivial scaling of these properties with polymer concentration by virtue of dimensional consistency with the property virial expansion[62,63].

We show an example of a "gel" of equilibrated tumbleweed domains in Figure 1 (d) where we see that individual tumbleweed domains, such as the highlighted one, become "invisible" once they start overlapping appreciably. (The same phenomena is apparent in heaps of real tumbleweeds[25]). As one interesting effect, we can expect the impingement of these deformable domains to lead to a kind of gel formation[64], as observed in recent studies of soft colloidal particles[65] and polymer melts containing star–like polymers[66,67]. Such gels, composed of tough but highly deformable domains, should lead to interesting applications and, indeed, polymer composites formed by multi–walled CNTs have already been shown to exhibit extremely promising material properties such as the flammability reduction of polymeric materials[68] and suppression of die–swell in extruded polymer materials[69], both effects deriving from CNT network formation within the polymer matrix, imparting a gel–like rheology to the material as a whole[69]. It would clearly be interesting to investigate these properties from a soft colloidal particle perspective rather than the dispersed rod paradigm that has formerly been emphasized in modeling CNT materials. By adopting more realistic models of CNT materials, it should then be possible to better realize, understand, and control the properties of this promising class of composite materials.

Although we have assumed a constancy of the CNT tumbleweed radius in our model calculations based on experimental observations, it would also be natural to assume a CNT tumbleweed model in which these structures continue growing by a random branching process as in true tumbleweeds, leading to a natural carbon nanotube growth structure having a dendrimer or hyperbranched polymer architecture. Such structures should also resemble the observed CNT morphologies rather well and lead to low conductivity percolation thresholds, screenings, etc., but we expect this type of morphologies to exhibit different mass scaling relationships for the intrinsic viscosity, chain radius of gyration, etc. Consistent with this possibility, there is some evidence from size exclusion chromatography [70] that nominal single wall carbon nanotube materials exhibit and intrinsic viscosity scaling with CNT particle mass consistent with compacts branched polymers. Further work is needed to understand the physical factors governing

the growth of these interesting carbonaceous particles, so that, the tumbleweed model can refined based on a firm observational data. X–ray, tomography imaging and neutron scattering over a large wavevector (length scale) range should be very helpful in resolving their internal structure.

4.1 Disclaimer

Certain commercial materials, equipment, or instruments were identified to specify experimental procedures. Such identification implies neither recommendation or endorsement by the National Institute of Standards and Technology nor that the materials or equipment identified were necessarily the best available for the purpose.

5 Acknowledgments

We thank Prof. Francis W. Starr and Dr. Alexandros Chremos from Wesleyan University and Dr. J Alexander Liddle from NIST for helpful discussions. We are also grateful to Dr. András Vládar and Dr. Tinh Nguyen from NIST for providing us with some of the images in Figure 1, i.e., panels (a) and (b), respectively. We thank Dr. Sen form Bhabha Atomic Research Centre for providing us the SANS data presented in Figure 5.

References

1 X.-L. Liu, H.-J. Lu and L.-Y. Xing, *J. Appl. Polym. Sci*, 2014, **131**, 1–7.
2 W. Bauhofer and J. Z. Kovacs, *Compos. Sci. Tech.*, 2009, **69**, 1486–1498.
3 D. Simien, J. A. Fagan, W. Luo, J. F. Douglas, K. Migler and J. Obrzut, *ACS Nano*, 2008, **2**, 1879–1884.
4 S. U. S. Choi, Z. G. Zhang, W. Yu, F. E. Lockwood and E. Grulke, *Appl. Phys. Lett.*, 2001, **79**, 2252.
5 M. Morcom, K. Atkinson and G. P. Simon, *Polymer*, 2010, **51**, 3540–3550.
6 Z. F. Ren, *Science*, 1998, **282**, 1105–1107.
7 C. Y. Khripin, X. Tu, J. M. Heddleston, C. Silvera-Batista, A. R. Hight Walker, J. Fagan and M. Zheng, *Anal. Chem.*, 2013, **85**, 1382–8.
8 M. Zheng and E. D. Semke, *J. Am. Chem. Soc.*, 2007, **129**, 6084–6085.
9 T. Chatterjee, A. Jackson and R. Krishnamoorti, *J. Am. Chem. Soc.*, 2008, **130**, 6934–6935.
10 G. R. Kasaliwal, S. Pegel, A. Göldel, P. Pötschke and G. Heinrich, *Polymer*, 2010, **51**, 2708–2720.
11 N. Grobert, *Mater. Today*, 2007, **10**, 28 – 35.
12 R. Schueler and J. Petermann, *J. Appl. Polym. Sci.*, 1997, 1741–1746.
13 S. Hofmann, R. Sharma, C. Ducati, G. Du, C. Mattevi, C. Cepek, M. Cantoro, S. Pisana, A. Parvez, F. Cervantes-Sodi, A. C. Ferrari, R. Dunin-Borkowski, S. Lizzit, L. Petaccia, A. Goldoni and J. Robertson, *Nano Lett.*, 2007, **7**, 602–608.
14 F. Garcia-Vidal, J. Pitarke and J. Pendry, *Phys. Rev. Lett.*, 1997, 4289–4292.
15 W.-S. Tung, V. Bird, R. J. Composto, N. Clarke and K. I. Winey, *Macromolecules*, 2013, **46**, 5345–5354.
16 R. M. Mutiso and K. I. Winey, *Prog. Polym. Sci.*, 2015, **40**, 63 – 84.
17 A. Einstein, *Annalen der Physik*, 1911, **34**, 591–592.
18 J. Maxwell, *A treatise on electricity and magnetism*, Dover Publications, 1954.
19 J. F. Douglas and E. J. Garboczi, *Intrinsic viscosity and the polarizability of particles having a wide range of shapes*, John Wiley & Sons, Inc., 2007, pp. 85–153.
20 E. J. Garboczi and J. F. Douglas, *Phys. Rev. E.*, 1996, **53**, 6169–6180.
21 M. Mansfield and J. Douglas, *Phys. Rev. E*, 2008, **78**, 046712.
22 *ZENO*, http://web.stevens.edu/zeno/.
23 A. Friedman and J. F. Douglas, *Mathematics in Industrial Problems*, Springer New York, 1995, vol. 67, pp. 166–185.
24 G. Pólya and G. Szegő, *Isoperimetric Inequalities in Mathematical Physics*, Princeton University Press, 1951.
25 *The morphology of actual tumbleweeds is ilustrated in :*, http://ngm.nationalgeographic.com/2013/12/tumbleweeds/cook-jenshel-photography/.
26 T. Nguyen, B. Pellegrin, C. Bernard, X. Gu, J. M. Gorham, P. Stutzman and D. Stanley, *J. Phys.: Conf. Ser.*, 2011, **304**, 012060.
27 *Accumulations of real tumbleweeds are shown in*, http://www.cbsnews.com/video/tumbleweeds-bury-new-mexico-town/.
28 H. Yamakawa, *Modern Theory of Polymer Solutions*, Harper & Row, 1971.
29 B. A. Pazmino Betancourt, J. F. Douglas and F. W. Starr, *Soft Matter*, 2013, **9**, 241–254.
30 S. T. Knauert, J. F. Douglas and F. W. Starr, *Macromolecules*, 2010, **43**, 3438–3445.
31 D. R. Heine, M. K. Petersen and G. S. Grest, *J. Chem. Phys.*, 2010, **132**, 184509.
32 G. Y. Slepyan, S. A. Maksimenko, A. Lakhtakia, O. Yevtushenko and A. V. Gusakov, *Phys. Rev. B*, 1999, **60**, 17136–17149.
33 M. Mansfield, J. Douglas and E. Garboczi, *Phys. Rev. E*, 2001, **64**, 061401.
34 J. E. Martin and G. Gulley, *J. Appl Phys.*, 2009, **106**, 1–7.
35 J. E. Martin, K. J. Solis, D. Rademacher and V. Raksha, *J.*

Appl Phys., 2012, **112**, –.
36 H. Lee, C. Yun, H. Kim and C. Lee, *J. Phys. Chem. C.*, 2007, **111**, 18882–18887.
37 N. Fakhri, D. A. Tsyboulski, L. Cognet, R. B. Weisman and M. Pasquali, *Proc. Natl. Acad. Sci U.S.A.*, 2009, **106**, 14219–14223.
38 D. McLachlan, W. Heiss, C. Chiteme and J. Wu, *Phys. Rev. B*, 1998, **58**, 13558–13564.
39 K. Kremer and G. S. Grest, *J. Chem. Phys.*, 1990, **92**, 5057–5086.
40 S. Kim, G. Mulholland and M. Zachariah, *Carbon*, 2009, **47**, 1297–1302.
41 S. Plimpton, *J. Comp. Phys.*, 1995, **117**, 1–19.
42 http://plasma-gate-weizmann.ac.il/Grace.
43 W. Humphrey, A. Dalke and K. Schulten, *J. Mol. Graphics*, 1996, **14**, 33–38.
44 M. L. Mansfield and J. F. Douglas, *Macromolecules*, 2008, **41**, 5412–5421.
45 J. F. Douglas, H.-X. Zhou and J. B. Hubbard, *Phys. Rev. E*, 1994, **49**, 5319–5331.
46 H.-X. Zhou, A. Szabo, J. F. Douglas and J. B. Hubbard, *J. Chem. Phys.*, 1994, **100**, 3821.
47 P. Debye and A. M. Bueche, *J. Chem. Phys.*, 1948, **16**, year.
48 J. Rauch, *Partial Differential Equations*, Springer New York, 1991.
49 J. Rauch and M. Taylor, *J. Math. Phys.*, 1975, **16**, year.
50 R. Zwanzig, *Proc. Natl. Acad. Sci U.S.A.*, 1990, **87**, 5856–5857.
51 H. T. Brown and F. Escombe, *Proc. R. Soc. of London*, 1900, **67**, pp. 124–128.
52 M. Laso, N. C. Karayiannis, K. Foteinopoulou, M. L. Mansfield and M. Kroger, *Soft Matter*, 2009, **5**, 1762–1770.
53 D. Stauffer and A. Aharony, *Introduction to Percolation Theory*, Taylor & Francis Ltd., 1992.
54 S. B. Kharchenko, J. F. Douglas, J. Obrzut, E. a. Grulke and K. B. Migler, *Nat. Mater.*, 2004, **3**, 564–568.
55 E. Petersen, T. Lam, J. Gorham, K. Scott, C. Long, R. Sharma, L. Sung, J. Liddle and T. Nguyen, *Nanotech*, 2014, **3**, 75–78.
56 D. W. Schaefer, J. Zhao, J. M. Brown, D. P. Anderson and D. W. Tomlin, *Chem. Phys. Lett.*, 2003, **375**, 369 – 375.
57 B. J. Bauer, E. K. Hobbie and M. L. Becker, *Macromolecules*, 2006, **39**, 2637–2642.
58 J. M. Brown, D. P. Anderson, R. S. Justice, K. Lafdi, M. Belfor, K. L. Strong and D. W. Schaefer, *Polymer*, 2005, **46**, 10854 – 10865.
59 Q. Chen, C. Saltiel, S. Manickavasagam, L. S. Schadler, R. W. Siegel and H. Yang, *Journal of Colloid and Interface Science*, 2004, **280**, 91 – 97.
60 D. Sen, K. Dasgupta, J. Bahadur, S. Mazumder and D. Sathiyamoorthy, *Pramana*, 2008, **71**, 971–977.
61 M. L. Mansfield and J. F. Douglas, *J. Chem. Phys.*, 2013, **139**, 044901.
62 P. de Gennes, *Scaling Concepts in Polymer Physics*, Cornell University Press, 1979.
63 K. J. Zhang, M. E. Briggs, R. W. Gammon, J. V. Sengers and J. F. Douglas, *J. Chem. Phys.*, 1999, **111**, year.
64 J. Bicerano, J. F. Douglas and D. A. Brune, *J. Macromol Sci., Part C: Polym. Rev.*, 1999, **39**, 561–642.
65 F. Di Lorenzo and S. Seiffert, *Macromolecules*, 2013, **46**, 1962–1972.
66 J. Stellbrink, J. Allgaier and D. Richter, *Phys. Rev. E*, 1997, **56**, R3772–R3775.
67 A. Chremos and A. Panagiotopoulos, *Phys. Rev. Lett.*, 2011, **107**, 105503.
68 T. Kashiwagi, F. Du, J. F. Douglas, K. I. Winey, R. H. Harris and J. R. Shields, *Nat. Mater.*, 2005, **4**, 928–933.
69 D.-H. Xu, Z.-G. Wang and J. F. Douglas, *Macromolecules*, 2008, **41**, 815–825.
70 B. J. Bauer, M. L. Becker, V. Bajpai, J. A. Fagan, E. K. Hobbie, K. Migler, C. M. Guttman and W. R. Blair, *The Journal of Physical Chemistry C*, 2007, **111**, 17914–17918.